

Midrange Affinity Fluorescent Zn(II) Sensors of the Zinpyr Family: Syntheses, Characterization, and Biological Imaging Applications

Elizabeth M. Nolan,[†] Jacek Jaworski,^{‡,§,⊥} Maryann E. Racine,[†] Morgan Sheng,^{‡,§,⊥,‡} and Stephen J. Lippard^{*,†}

Departments of Chemistry and Brain and Cognitive Sciences, Picower Institute of Learning and Memory, RIKEN-MIT Neuroscience Research Center, and Howard Hughes Medical Institute, Massachusetts Institute of Technology, Cambridge, Massachusetts 02139

Received June 22, 2006

The syntheses and photophysical characterization of ZP9, 2-{2-chloro-6-hydroxy-3-oxo-5-[(2-{[pyridin-2-ylmethyl-(1*H*-pyrrol-2-ylmethyl)amino]methyl}phenylamino)methyl]-3*H*-xanthen-9-yl}benzoic acid, and ZP10, 2-{2-chloro-6-hydroxy-5-[(2-{[(1-methyl-1*H*-pyrrol-2-ylmethyl)pyridin-2-ylmethylamino]methyl}phenylamino)methyl]-3-oxo-3*H*-xanthen-9-yl}benzoic acid, two asymmetrically derivatized fluorescein-based dyes, are described. These sensors each contain an aniline-based ligand moiety functionalized with a pyridyl-amine-pyrrole group and have dissociation constants for Zn(II) in the sub-micromolar (ZP9) and low-micromolar (ZP10) range, which we define as “midrange”. They give ~12- (ZP9) and ~7-fold (ZP10) fluorescence turn-on immediately following Zn(II) addition at neutral pH and exhibit improved selectivity for Zn(II) compared to the di-(2-picolyl)amine-based Zinpyr (ZP) sensors. Confocal microscopy studies indicate that such asymmetrical fluorescein-based probes are cell permeable and Zn(II) responsive in vivo.

Introduction

Many factors determine the performance of small molecule sensors in vivo, including their photophysical properties, sensitivity, and selectivity for the analyte of interest, affinity for the analyte and other species in the biological milieu, and behavior and localization within cells or tissues. Some of these features, such as emission profiles and binding affinity, are relatively easy to control, whereas those pertaining to performance in a given biological sample often cannot be readily anticipated prior to a first series of experiments. The work described here focuses on several of these issues in the context of fluorescent Zn(II) sensor design and biological application.

It is of general interest to procure Zn(II) sensors that have similar photophysical properties and span a range of dissociation constants.^{1–6} Such molecules are invaluable for

studies in neurobiology, where estimated concentrations of Zn(II) range from pico- to sub-millimolar depending on the cell type and phenomena under investigation.^{7–9} Many small-molecule Zn(II) sensors use the di-(2-picolyl)amine (DPA) ligand fragment,^{10–28} which affords selectivity for Zn(II) over high concentrations of K(I), Na(I), Ca(II), and Mg(II) and

- (3) Gee, K. R.; Zhou, Z.-L.; Ton-That, D.; Sensi, S. L.; Weiss, J. H. *Cell Calcium* **2002**, *31*, 245–251.
- (4) Shults, M. D.; Pearce, D. A.; Imperiali, B. *J. Am. Chem. Soc.* **2003**, *125*, 10591–10597.
- (5) Henary, M. M.; Wu, Y.; Fahrni, C. J. *Chem. Eur. J.* **2004**, *10*, 3015–3025.
- (6) Komatsu, K.; Kikuchi, K.; Kojima, H.; Urano, Y.; Nagano, T. *J. Am. Chem. Soc.* **2005**, *127*, 10197–10204.
- (7) Frederickson, C. J. *Int. Rev. Neurobiol.* **1989**, *31*, 145–238.
- (8) Frederickson, C. J.; Koh, J.-H.; Bush, A. I. *Nat. Neurosci.* **2005**, *6*, 449–462.
- (9) Bozym, R. A.; Thompson, R. B.; Stoddard, A. K.; Fierke, C. A. *ACS Chem. Biol.* **2006**, *1*, 103–111.
- (10) de Silva, S. A.; Zavaleta, A.; Baron, D. E.; Allam, O.; Isidor, E. V.; Kashimura, N.; Percarpio, J. M. *Tetrahedron Lett.* **1997**, *38*, 2237–2240.
- (11) Hirano, T.; Kikuchi, K.; Urano, Y.; Higuchi, T.; Nagano, T. *J. Am. Chem. Soc.* **2000**, *122*, 12399–12400.
- (12) Hirano, T.; Kikuchi, K.; Urano, Y.; Nagano, T. *J. Am. Chem. Soc.* **2002**, *124*, 6555–6562.
- (13) Maruyama, S.; Kikuchi, K.; Hirano, T.; Urano, Y.; Nagano, T. *J. Am. Chem. Soc.* **2002**, *124*, 10650–10651.
- (14) Kiyose, K.; Kojima, H.; Urano, Y.; Nagano, T. *J. Am. Chem. Soc.* **2006**, *128*, 6548–6549.
- (15) Kim, T. W.; Park, J.-H.; Hong, J.-I. *J. Chem. Soc., Perkin Trans. 2* **2002**, 923–927.

* To whom correspondence should be addressed. E-mail: lippard@mit.edu.

[†] Department of Chemistry.

[‡] Department of Brain and Cognitive Sciences.

[§] Picower Institute of Learning and Memory.

^{||} RIKEN-MIT Neuroscience Research Center.

[⊥] Howard Hughes Medical Institute.

- (1) Chang, C. J.; Lippard, S. J. In *Neurodegenerative Diseases and Metal Ions*; Metal Ions in Life Sciences, Vol. 1; Sigel, A., Sigel, H., Sigel, R. K. O., Eds.; Wiley: New York, 2006; pp 321–370.
- (2) Fierke, C. A.; Thompson, R. B. *BioMetals* **2001**, *14*, 205–222.

is therefore suitable for biological work. Because DPA itself binds Zn(II) with nanomolar affinity at pH 7,^{29,30} alternative Zn(II)-binding frameworks are required to raise the apparent dissociation constant (K_d). Several strategies have been employed to achieve this objective. A series of ratiometric probes that employ the benzimidazole reporting group were described in which the Zn(II) binding affinity was tuned over the sub-picomolar to micromolar range.⁵ Systematic modification of the DPA-based ligand employed in ZnAF-1 and ZnAF-2 afforded a sensor family with similar photophysical properties, fast association rates, and dissociation constants for Zn(II) that vary by approximately 6 orders of magnitude.⁶ Substitution of the pyridyl groups in Zinpyr-1¹⁹ with 6-methylpyridyl moieties effectively raised the apparent ZP1/Zn(II) K_{d1} value from the sub-nanomolar to the sub-micromolar.³¹ Other departures from the DPA ligand were incorporated in the design of the Zinspy (ZS)³² and QZ³³ sensor families; the latter probes exhibit micromolar dissociation constants. Modulation of Zn(II) affinity has also been considered in the design of protein-² and peptide-based sensors.⁴ Several of these probes have been employed for biological imaging and provide definitive proof that binding affinity is an important parameter for in vivo Zn(II) detection.^{6,33}

Our laboratory has prepared fluorescein-based Zn(II) sensors with a single Zn(II) binding unit installed on the xanthene moiety (Figure 1).^{21,26,27,32,33} In the present work, we have modified the sensor platform of ZP4, **1**, through pyrrole-for-pyridyl substitution and have evaluated the effects of this variation on both the photophysical and metal-binding properties. We anticipated that incorporation of pyrrole or *N*-methylpyrrole, both of which are poor bases, would raise the Zn(II) dissociation constant relative to that of the parent compound ZP4 ($K_d = 0.65$ nM), which contains the DPA

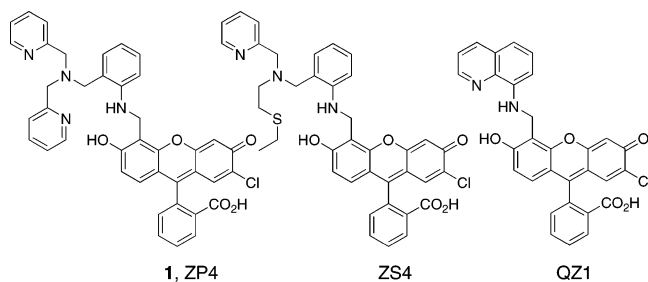


Figure 1. Examples of asymmetrical fluorescein-based Zn(II) sensors of the Zinpyr, Zinspy, and QZ families.

chelate, while maintaining similar fluorescence properties. Sensors ZP9, **2**, and ZP10, **3**, (Scheme 1) give fluorescence enhancement immediately following Zn(II) coordination, have dissociation constants for Zn(II) in the sub- (ZP9) to low-micromolar (ZP10) range, and exhibit improved metal-binding selectivity for Zn(II) compared to DPA-based ZP²¹ and thioether-containing ZS sensors.³² We also investigated the utility of aniline-based ZP probes for select biological imaging applications. On the basis of previous investigations with ZP4, which revealed that it selectively stains dead or damaged neurons, thereby suggesting cell impermeability,^{21,34} we expected that ZP9 and ZP10 would also be cell impermeable without modification. Preliminary observations indicated otherwise, and an account of our more detailed cellular studies with ZP9 and ZP4 is provided here.

Experimental Section

Reagents. Acetonitrile was purged with Ar and dried by passage through columns of Al₂O₃. Anhydrous EtOAc and 1,2-dichloroethane (DCE) were purchased from Aldrich and used as received. In preparation for the syntheses of amines **4** and **5**, ethanol and methanol were dried over MgSO₄. *N*-(2-Pyridylmethyl)-*N*-(1*H*-2-pyrrolylmethyl)amine,³⁵ **4**, and 7'-chloro-4'-fluoresceincarboxaldehyde,²⁶ **6**, were synthesized according to literature procedures. All other reagents were obtained from Aldrich and used as received.

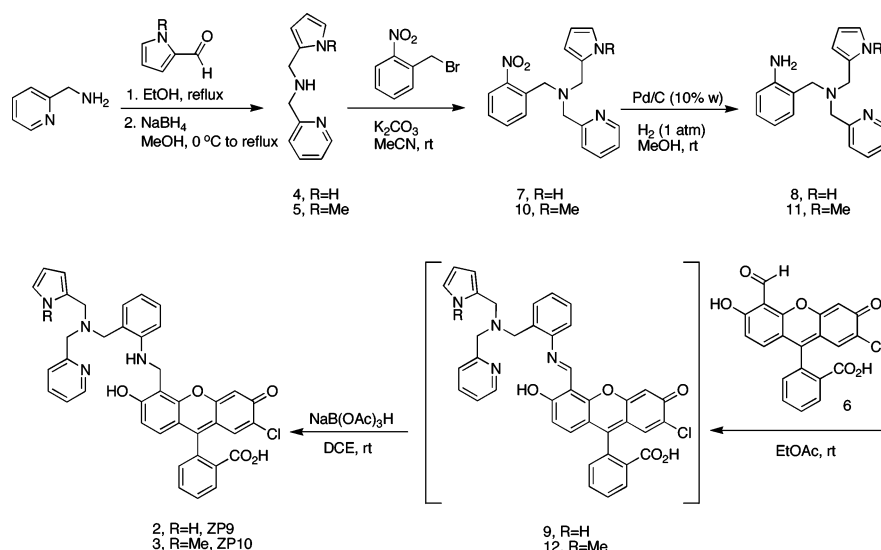
General Methods. Analytical TLC was performed on Merck F254 silica gel plates, Merck F254 aluminum oxide plates, or octadecyl-functionalized (reverse phase, RP18) plates (0.25 mm thickness). Reverse-phase plates of 1 mm thickness manufactured by EM Science were used for preparative TLC. NMR spectra were obtained on a Varian 300 MHz spectrophotometer operating at ambient probe temperature, 283 K. Both ¹H and ¹³C NMR spectra were referenced to internal probe standards. An Avatar FTIR instrument was used to obtain IR spectra. High-resolution mass spectrometry was performed by staff at the MIT Department of Chemistry Instrumentation Facility.

(2-Nitrobenzyl)pyridin-2-ylmethyl-(1*H*-pyrrol-2-ylmethyl)amine (7). Portions of 2-nitrobenzylbromide (533 mg, 2.47 mmol), **4** (502 mg, 2.47 mmol), K₂CO₃ (400 mg, 2.89 mmol), and activated 3 Å molecular sieves were combined in 20 mL of MeCN and stirred vigorously overnight at room temperature. The reaction mixture was filtered through Celite, and the solvent was removed under reduced pressure to yield a brown-yellow oil. The crude product

- (16) Lim, N. C.; Brückner, C. *Chem. Commun.* **2004**, 1094–1095.
 (17) Lim, N. C.; Schuster, J. V.; Porto, M. C.; Tanudra, M. A.; Yao, L.; Freake, H. C.; Brückner, C. *Inorg. Chem.* **2005**, *44*, 2018–2030.
 (18) Wu, Y.; Peng, X.; Guo, B.; Fan, J.; Zhang, Z.; Wang, J.; Cui, A.; Gao, Y. *Org. Biomol. Chem.* **2005**, *3*, 1387–1392.
 (19) Walkup, G. K.; Burdette, S. C.; Lippard, S. J.; Tsien, R. Y. *J. Am. Chem. Soc.* **2000**, *122*, 5644–5645.
 (20) Burdette, S. C.; Walkup, G. K.; Spingler, B.; Tsien, R. Y.; Lippard, S. J. *J. Am. Chem. Soc.* **2001**, *123*, 7831–7841.
 (21) Burdette, S. C.; Frederickson, C. J.; Bu, W.; Lippard, S. J. *J. Am. Chem. Soc.* **2003**, *125*, 1778–1787.
 (22) Chang, C. J.; Nolan, E. M.; Jaworski, J.; Burdette, S. C.; Sheng, M.; Lippard, S. J. *Chem. Biol.* **2004**, *11*, 203–210.
 (23) Woodroffe, C. C.; Masalha, R.; Barnes, K. R.; Frederickson, C. J.; Lippard, S. J. *Chem. Biol.* **2004**, *11*, 1659–1666.
 (24) Woodroffe, C. C.; Lippard, S. J. *J. Am. Chem. Soc.* **2003**, *125*, 11458–11459.
 (25) Woodroffe, C. C.; Won, A. C.; Lippard, S. J. *Inorg. Chem.* **2005**, *44*, 3112–3120.
 (26) Nolan, E. M.; Burdette, S. C.; Harvey, J. H.; Hilderbrand, S. A.; Lippard, S. J. *Inorg. Chem.* **2004**, *43*, 2624–2635.
 (27) Chang, C. J.; Nolan, E. M.; Jaworski, J.; Okamoto, K.-I.; Hayashi, Y.; Sheng, M.; Lippard, S. J. *Inorg. Chem.* **2004**, *43*, 6774–6779.
 (28) Chang, C. J.; Jaworski, J.; Nolan, E. M.; Sheng, M.; Lippard, S. J. *Proc. Natl. Acad. Sci. U.S.A.* **2004**, *101*, 1129–1134.
 (29) Anderegg, G.; Hubmann, E.; Podder, N. G.; Wenk, F. *Helv. Chim. Acta* **1977**, *60*, 123–140.
 (30) Gruenwedel, D. W. *Inorg. Chem.* **1968**, *7*, 495–501.
 (31) Goldsmith, C. R.; Lippard, S. J. *Inorg. Chem.* **2006**, *45*, 555–561.
 (32) Nolan, E. M.; Lippard, S. J. *Inorg. Chem.* **2004**, *43*, 8310–8317.
 (33) Nolan, E. M.; Jaworski, J.; Okamoto, K.-I.; Hayashi, Y.; Sheng, M.; Lippard, S. J. *J. Am. Chem. Soc.* **2005**, *127*, 16812–16823.

- (34) Frederickson, C. J.; Burdette, S. C.; Frederickson, C. J.; Sensi, S. L.; Weiss, J. H.; Yin, H. Z.; Balaji, R. V.; Truong-Tran, A. Q.; Bedell, E.; Prough, D. S.; Lippard, S. J. *J. Neurosci. Methods* **2004**, *139*, 79–89.
 (35) de Bruin, B.; Kicken, R. J. N. A. M.; Suos, N. F. A.; Donners, M. P. J.; den Reijer, C. J.; Sandee, A. J.; de Gelder, R.; Smits, J. M. M.; Gal, A. W.; Spek, A. L. *Eur. J. Inorg. Chem.* **1999**, 1581–1592.

Scheme 1. Syntheses of ZP9 and ZP10



was flushed through a plug of Al_2O_3 (5:1 $\text{CH}_2\text{Cl}_2/\text{EtOAc}$), which yielded a light-yellow solid (730 mg, 91%). TLC: $R_f = 0.58$ (Al_2O_3 , 2:1 hexanes/ EtOAc). mp: 85–86 °C. ^1H NMR (CDCl_3 , 300 MHz): δ 3.42 (2H, s), 3.68 (2H, s), 4.00 (2H, s), 6.04 (1H, m), 6.19 (1H, m), 6.88 (1H, m), 7.21 (1H, m), 7.33–7.43 (2H, m), 7.44–7.53 (2H, m), 7.54–7.77 (2H, m), 8.56 (1H, dq), 9.98 (1H, br s). ^{13}C NMR (CDCl_3 , 125 MHz): δ 48.06, 55.69, 58.85, 107.64, 108.52, 117.88, 122.43, 124.30, 124.85, 126.87, 128.16, 131.38, 132.07, 134.25, 136.92, 148.35, 150.34, 158.51. FTIR (KBr, cm^{-1}): 3426 (m), 3198 (w), 3077 (w), 2970 (w), 2920 (m), 1595 (m), 1570 (m), 1528 (s), 1470 (m), 1442 (m), 1431 (m), 1413 (w), 1362 (s), 1300 (w), 1259 (w), 1243 (w), 1231 (w), 1151 (w), 1132 (w), 1114 (m), 1103 (m), 1079 (w), 1051 (w), 1029 (w), 1001 (w), 991 (m), 965 (w), 952 (w), 884 (m), 866 (w), 812 (m), 782 (m), 768 (m), 732 (s), 676 (s), 632 (w), 610 (w). HRMS (ESI): calcd $[\text{M} + \text{Na}]^+$, 345.1322; found, 345.1338.

2-[[Pyridin-2-ylmethyl-(1H-pyrrol-2-ylmethyl)amino]methyl]-phenylamine (8). A flask containing Pd/C (10% activated, 180 mg) was purged with Ar, and 10 mL of MeOH was added. A portion (101 mg, 0.313 mmol) of **7** dissolved in 15 mL of MeOH was added, and a balloon filled with H_2 was attached. The reaction mixture was stirred vigorously under H_2 for 2.5 h, purged with Ar, and filtered through Celite before the solvent was removed under reduced pressure. Flash chromatography on Al_2O_3 using a solvent gradient (10:1–4:1 $\text{CH}_2\text{Cl}_2/\text{EtOAc}$ with 1% $^i\text{PrNH}_2$) yielded the purified product as a brown oil (48 mg, 52%). TLC: $R_f = 0.43$ (Al_2O_3 , 2:1 hexanes/ EtOAc). ^1H NMR (CDCl_3 , 300 MHz): δ 3.57 (2H, s), 3.69 (2H, s), 3.71 (2H, s), 4.95 (2H, br s), 6.07 (1H, m), 6.18 (1, m), 6.67 (2H, m), 6.85 (1H, m), 7.09 (2H, m), 7.32 (2H, m), 7.69 (1H, td), 8.62 (1H, dq), 10.23 (1H, br s). ^{13}C NMR (CDCl_3 , 125 MHz): δ 47.92, 58.02, 58.10, 107.77, 108.33, 115.73, 117.48, 117.64, 122.41, 122.57, 124.61, 127.36, 128.47, 130.93, 136.86, 147.05, 148.75, 158.84. FTIR (NaCl disk, cm^{-1}): 3403 (m), 3298 (m), 3092 (w), 3011 (w), 2922 (w), 2832 (m), 1656 (w), 1614 (s), 1592 (s), 1569 (m), 1494 (s), 1475 (m), 1461 (m), 1435 (m), 1405 (w), 1366 (m), 1339 (w), 1315 (w), 1297 (w), 1284 (w), 1261 (w), 1236 (w), 1150 (m), 1114 (m), 1091 (m), 1049 (w), 1027 (m), 997 (w), 980 (w), 970 (w), 956 (w), 926 (w), 884 (w), 841 (w), 801 (m), 751 (s), 720 (s), 640 (w), 615 (w), 560 (w), 540 (w), 500 (w). HRMS (ESI): calcd $[\text{M} + \text{Na}]^+$, 315.1580; found, 315.1575.

2-[2-Chloro-6-hydroxy-3-oxo-5-[(2-[[pyridin-2-ylmethyl-(1H-pyrrol-2-ylmethyl)amino]methyl]phenylamino)methyl]-3H-xanthen-9-yl]benzoic Acid (2, Zinpyr-9, ZP9). Portions of **8** (75

mg, 0.25 mmol) and **6** (72 mg, 0.26 mmol) were combined in 10 mL of EtOAc , and the mixture was stirred overnight at room temperature. The solution turned deep red. The solvent was removed under reduced pressure, and the red residue, intermediate **9**, was suspended in 5 mL of 1,2-dichloroethane. A portion (160 mg, 0.754 mmol) of $\text{NaB}(\text{OAc})_3\text{H}$ was added, and the reaction mixture was stirred at room temperature. The solution became clear and light orange over the course of 3 h. Preparative TLC on reverse phase silica gel (6:1 $\text{MeOH}/0.1 \text{ N HCl}$) yielded the pure product as a red solid (42 mg, 33%). This material can also be purified by preparative TLC on silica gel (20:1 $\text{CHCl}_3/\text{MeOH}$). TLC: $R_f = 0.41$ (RP silica, 6:1 $\text{MeOH}/0.1 \text{ N HCl}$). mp (dec): >325 °C. ^1H NMR (CD_3OD , 300 MHz): δ 3.56–3.67 (6H, m), 4.57 (2H, s), 5.93 (2H, d), 6.63–6.73 (4H, m), 6.81 (1H, s), 6.99–7.24 (6H, m), 7.39 (1H, t), 7.71–7.83 (3H, m), 8.06 (1H, d), 8.26 (1H, d). FTIR (KBr, cm^{-1}): 3418 (s), 3050 (w), 2920 (m), 2850 (m), 1761 (s), 1632 (m), 1606 (s), 1582 (s), 1516 (m), 1490 (m), 1451 (s), 1368 (m), 1282 (s), 1252 (m), 1218 (m), 1149 (s), 1109 (m), 1091 (m), 1070 (m), 1025 (w), 1008 (m), 874 (w), 834 (w), 798 (w), 751 (m), 722 (m), 702 (m), 621 (w), 597 (w), 549 (w), 470 (m). HRMS (ESI): calcd $[\text{M} - \text{H}]^-$, 669.1910; found, 669.1902.

(1-Methyl-1H-pyrrol-2-ylmethyl)pyridin-2-ylmethylamine (5). *N*-Methyl-2-pyrrolicarboxaldehyde (2.0 g, 18.3 mmol) was dissolved in 25 mL of EtOH with stirring. A portion (2.0 g, 18.5 mmol) of 2-(aminomethyl)pyridine was added dropwise to the stirred solution, which was refluxed for 30 min. The resulting yellow solution was cooled, and the solvent was removed in vacuo to yield an orange oil. The oil was dissolved in 40 mL of MeOH, and the solution was cooled to 0 °C. A portion (770 mg, 20.5 mmol) of NaBH_4 was added, and the reaction mixture was stirred at 0 °C for 30 min and then warmed to room temperature. After it was stirred for an additional 30 min, the solution was heated to reflux for 4 h and cooled. The solvent was removed under reduced pressure, and the resulting yellow-white residue was dissolved in 20 mL of water, which was extracted with Et_2O (3 \times 20 mL). The combined organics were dried over MgSO_4 , and the solvent was removed in vacuo, which yielded the product as a yellow oil (3.1 g, 82%). TLC: $R_f = 0.44$ (silica, 9:1 $\text{CHCl}_3/\text{MeOH}$). ^1H NMR (CDCl_3 , 300 MHz): δ 2.15 (1H, br s), 3.64 (3H, s), 3.77 (2H, s), 3.93 (2H, s), 6.04 (2H, d), 6.58 (1H, t), 7.16 (1H, m), 7.31 (1H, d), 7.64 (1H, td), 8.55 (1H, dq). ^{13}C NMR (CDCl_3 , 125 MHz): δ 33.87, 45.05, 54.50, 106.56, 108.28, 122.04, 122.46, 122.50, 130.95, 136.53, 149.37, 159.97. FTIR (NaCl disk, cm^{-1}): 3315 (m, br), 3090 (w),

3064 (w), 3007 (m), 2920 (m), 2828 (m), 1591 (s), 1569 (s), 1496 (s), 1473 (s), 1456 (m), 1433 (s), 1416 (m), 1356 (w), 1325 (w), 1300 (s), 1261 (w), 1215 (w), 1182 (w), 1170 (w), 1147 (w), 1113 (m), 1088 (s), 1049 (m), 1014 (w), 994 (m), 955 (w), 938 (w), 917 (w), 890 (w), 845 (m), 794 (m), 758 (s), 710 (s), 626 (m), 611 (m). HRMS (ESI): calcd $[M + Na]^+$, 224.1158; found, 224.1151.

(1-Methyl-1H-pyrrol-2-ylmethyl)-(2-nitrobenzyl)pyridin-2-ylmethylamine (10). 2-Nitrobenzylbromide (1.07 g, 4.95 mmol), K_2CO_3 (1.36 g, 9.84 mmol), **5** (1.00 g, 4.97 mmol), and activated 3 Å molecular sieves were combined in 50 mL of MeCN, and the yellow solution was stirred vigorously at room temperature for 10 h. The mixture was filtered through Celite, and the solvent was removed under reduced pressure. Chromatography on silica gel (2:1 hexanes/EtOAc) afforded the purified product as light yellow solid after drying in vacuo (1.50 g, 89%). TLC: $R_f = 0.32$ (silica, 1:1 hexanes/EtOAc). mp: 89–91 °C. 1H NMR ($CDCl_3$, 300 MHz): δ 3.42 (3H, s), 3.56 (2H, s), 3.68 (2H, s), 3.99 (2H, s), 5.99 (1H, m), 6.07 (1H, m), 6.53 (1H, m), 7.12 (1H, td), 7.25 (1H, m), 7.34 (1H, td), 7.46 (1H, td), 7.50–7.63 (2H, m), 7.76 (1H, dd), 8.49 (1H, dq). ^{13}C NMR ($CDCl_3$, 125 MHz): δ 33.78, 51.15, 55.85, 60.71, 106.53, 110.43, 122.13, 122.94, 123.43, 124.41, 128.00, 128.59, 131.81, 132.35, 134.58, 136.40, 148.88, 150.06, 159.16. FTIR (KBr, cm^{-1}): 3103 (w), 3071 (w), 3006 (w), 2916 (w), 2878 (w), 2807 (m), 2792 (m), 2722 (w), 1608 (m), 1590 (m), 1568 (m), 1515 (s), 1489 (m), 1470 (m), 1434 (m), 1421 (m), 1375 (m), 1367 (m), 1356 (m), 1334 (s), 1298 (s), 1283 (m), 1261 (m), 1217 (m), 1185 (m), 1146 (m), 1117 (s), 1094 (m), 1073 (w), 1047 (m), 1013 (w), 1000 (m), 983 (m), 968 (m), 954 (m), 895 (m), 886 (w), 871 (w), 856 (w), 847 (w), 795 (m), 764 (s), 739 (s), 725 (s), 689 (m), 676 (w), 652 (w), 632 (w), 617 (m), 600 (w), 511 (w), 481 (w), 436 (w). HRMS (ESI): calcd $[M + Na]^+$, 337.1659; found, 337.1666.

2-[(1-Methyl-1H-pyrrol-2-ylmethyl)pyridin-2-ylmethylamino]methyl]phenylamine (11). Palladium on carbon (10% activated, 900 mg) was placed in a flask purged with Ar. A 20 mL solution of **10** (600 mg, 1.78 mmol) in 19:1 MeOH/ CH_2Cl_2 was added with a syringe. The mixture was stirred vigorously, and a balloon of H_2 was attached. After 1.5 h of stirring under H_2 , the reaction was purged with Ar, filtered through Celite, and the solvents were removed under reduced pressure. Column chromatography on Al_2O_3 (2:1–1:1 hexanes/EtOAc) yielded the purified product as an off-white solid (325 mg, 60%). TLC: $R_f = 0.47$ (silica, 2:1 hexanes/EtOAc). mp: 105–109 °C. 1H NMR ($CDCl_3$, 300 MHz): δ 3.40 (3H, s), 3.57 (2H, s), 3.61 (2H, s), 3.73 (2H, s), 4.53 (2H, br s), 6.04 (1H, t), 6.12 (1H, m), 6.54 (1H, m), 6.11–6.73 (2H, m), 7.06–7.20 (4H, m), 7.60 (1H, td), 8.56 (1H, dq). ^{13}C NMR ($CDCl_3$, 125 MHz): δ 33.57, 50.11, 57.74, 59.80, 106.62, 110.33, 115.48, 117.46, 122.10, 122.70, 123.75, 128.60, 129.13, 131.42, 136.34, 146.80, 149.12, 159.57. FTIR (KBr, cm^{-1}): 3456 (s), 3311 (m), 3231 (w), 3199 (w), 3022 (w), 2923 (m), 2886 (m), 2832 (m), 2809 (m), 1713 (w), 1630 (s), 1605 (m), 1591 (m), 1578 (m), 1567 (m), 1493 (s), 1475 (m), 1461 (m), 1445 (m), 1431 (m), 1413 (m), 1370 (m), 1358 (m), 1326 (m), 1310 (m), 1298 (m), 1267 (m), 1250 (w), 1221 (w), 1207 (w), 1180 (w), 1146 (m), 1109 (m), 1099 (m), 1081 (m), 1049 (w), 1035 (w), 997 (m), 968 (m), 954 (m), 934 (m), 897 (w), 887 (w), 869 (m), 866 (m), 837 (w), 790 (m), 770 (m), 752 (s), 724 (s), 682 (w), 633 (w), 612 (m), 548 (w), 516 (m), 466 (w), 444 (w), 410 (w). HRMS (ESI): calcd $[M + H]^+$, 307.1917; found, 307.1915.

2-[2-Chloro-6-hydroxy-5-[(2-[(1-methyl-1H-pyrrol-2-ylmethyl)pyridin-2-ylmethylamino]methyl]phenylamino)methyl]-3-oxo-3H-xanthen-9-yl]benzoic Acid (3, Zinpyr-10, ZP10). Portions of 7'-chloro-4'-fluoresceincarboxaldehyde (**6**, 75 mg, 0.19 mmol) and **11** (58 mg, 0.19 mmol) were combined in 5 mL of

EtOAc, and the mixture was stirred overnight at room temperature. The intermediate imine, **12**, precipitated as a peach-colored solid, and the mixture was cooled on ice and filtered. The precipitate was suspended in 5 mL of DCE, and $NaB(OAc)_3H$ (40 mg, 0.19 mmol) was added. Over the course of 3 h, the reaction became dark pink and clear and then turned light orange. Preparative TLC on reverse-phase silica gel (10:1 MeOH/0.1 N HCl) yielded the product as an orange solid (38 mg, 29%). mp (dec): >300 °C. 1H NMR ($CD_3OD/CDCl_3$, 300 MHz): δ 3.12 (3H, s), 3.48–3.64 (6H, m), 4.45 (2H, m), 5.65 (1H, m), 5.84 (1H, m), 6.23 (1H, m), 6.56–6.64 (3H, m), 6.97–7.12 (4H, d), 7.16–7.28 (3H, m), 7.29 (1H, d), 7.48 (1H, td), 7.60 (2H, m), 8.06 (1H, m), 8.24 (1H, d). FTIR (KBr, cm^{-1}): 3425 (s, br), 3062 (w), 2963 (m), 2921 (s), 2851 (m), 1763 (s), 1628 (m), 1605 (s), 1583 (s), 1519 (m), 1494 (m), 1450 (s), 1367 (m), 1282 (s), 1260 (s), 1216 (m), 1149 (m), 1106 (m), 1089 (m), 1070 (m), 1011 (m), 872 (m), 797 (m), 756 (m), 702 (m), 613 (w), 597 (w), 546 (w), 509 (w), 470 (w), 409 (w). HRMS (ESI): calcd $[M - H]^-$, 683.2056; found, 683.2047.

2-(2-Chloro-6-hydroxy-3-oxo-5-phenylaminomethyl-3H-xanthen-9-yl)benzoic Acid (13). Fluorescein carboxaldehyde **6** (38 mg, 0.097 mmol) and aniline (12 mg, 0.13 mmol) were added to 3 mL of EtOAc, and the resulting orange solution was stirred overnight at room temperature. The solvent was removed under reduced pressure, which gave a red-magenta residue. The residue was dissolved in 5 mL of 1,2-dichloroethane, and $NaB(OAc)_3H$ (24 mg, 0.11 mmol) was added. The cloudy orange solution was stirred overnight at room temperature, diluted with 15 mL of $CHCl_3$, washed with water (3×15 mL), and dried in vacuo. Preparative TLC of the crude material on silica gel (10:1 $CHCl_3/MeOH$) gave pure **3** as a magenta solid (8.5 mg, 18%). TLC: $R_f = 0.53$ (silica, 9:1 $CHCl_3/MeOH$). mp (dec): >300 °C. 1H NMR (CD_3OD , 500 MHz): δ 4.48–4.59 (2H, q), 6.54 (1H, d), 6.61 (1H, t), 6.73 (1H, m), 6.86 (2H, d), 7.00 (1H, d), 7.08–7.13 (3H, m), 7.19 (1H, d), 7.56 (2H, qd), 8.03 (1H, dd). FTIR (KBr, cm^{-1}): 3426 (m, br), 2960 (m), 2924 (s), 2854 (m), 1728 (w), 1638 (m), 1605 (m), 1575 (m), 1503 (m), 1461 (m), 1376 (m), 1341 (m), 1301 (m), 1261 (s), 1222 (w), 1186 (w), 1147 (m), 1096 (m), 1014 (m), 963 (w), 936 (w), 881 (w), 823 (s), 802 (s), 749 (m), 715 (m), 690 (m), 662 (w), 623 (m), 598 (m), 547 (m), 499 (w). HRMS (ESI) calcd $[M + H]^+$, 472.0946; found, 472.0930.

General Spectroscopic Procedures. Millipore water was used to prepare all aqueous solutions. PIPES, piperazine-*N,N'*-bis(2-ethanesulfonic acid), and 99.999% KCl were purchased from Calbiochem. Except for the pK_a titrations, measurements were made at pH 7 in 50 mM PIPES, 100 mM KCl buffer. Rigorously treating this buffer with Chelex (BioRad, manufacturer protocol) to remove any potential metal-ion contamination had negligible effect on the emission and Zn(II) response of ZP9 and ZP10 compared to that observed in untreated buffer. Aqueous Zn(II) stock solutions (100 mM) were prepared from anhydrous 99.999% $ZnCl_2$ obtained from Aldrich. DMSO stock solutions (1 mM) of ZP9 and ZP10 were prepared, partitioned, stored at -25 °C, and thawed in the dark before use. After dilution to the appropriate concentration, solutions for spectroscopic measurements contained 0.1 (1 μM dye solution, fluorescence) to 1% (10 μM dye solution, absorption) DMSO. A starting solution of 10 mM KOH and 100 mM KCl (pH ~ 12) was used for pH titrations. Quantum yields were measured relative to fluorescein in 0.1 N NaOH ($\Phi = 0.95$)³⁶ with excitation provided at 497 (ZP9, ZP10), 496 (compound **13**), 494 (Zn(II)-bound ZP10), or 493 (Zn(II)-bound ZP9) nm. Extinction coefficients were determined over a concentration range of 10–1 μM for apo ZP9

(36) Brannon, J. H.; Madge, D. *J. Phys. Chem.* **1978**, *82*, 705–709.

and ZP10 and from 5–1 μM for the corresponding Zn(II) complexes because of limited solubility at higher concentrations. Metal ion selectivity experiments were conducted as previously described.²⁶ Controls with ZP1, which preferentially binds Fe(II) over Zn(II), were conducted to test the aqueous Fe(II) solutions. All reported data are the averages of at least three independent measurements obtained using material from two independent syntheses. Further experimental details are available elsewhere.^{20,26}

Dissociation Constant Determination. The apparent zinc dissociation constants for ZP9 and ZP10 were determined by fluorimetric analysis. In a typical experiment, a 1 μM solution of the ZP compound was prepared (50 mM PIPES, 100 mM KCl, pH 7, Chelexed), and its emission spectrum was recorded. Various aliquots of 1 or 10 mM aqueous ZnCl₂ solutions were added, and the emission changes were noted. Excitation was provided at 497 nm, and the data were integrated from 505 to 650 nm, normalized, and plotted against the total concentration of Zn(II) in solution. The data were fit to a 1:1 metal/ligand model.³⁷

Stopped-Flow Fluorescence Studies. Single-mixing stopped-flow kinetics studies were performed with a Hi-Tech SF-61 DX2 double-mixing stopped-flow apparatus equipped with a fluorescence detector. Excitation was provided at 495 nm, and a GG495 glass cutoff filter (<455 nm) was placed over the exit to the photomultiplier tube. Emission was monitored from 455 to 700 nm. All solutions were prepared in 50 mM PIPES, 100 mM KCl, pH 7. Conditions for pseudo-first-order kinetics were maintained by using at least a 10-fold excess of Zn(II) in all experiments. With the exception of the temperature-dependent studies, all measurements were conducted at 4.3 ± 0.1 °C, maintained with a circulating bath. The temperature inside the sample chamber was monitored with an internal thermocouple. A series of control experiments were conducted where the initial ZP concentration was varied from 0.5 to 5 μM after mixing to ensure that the observed rate constant was independent of initial dye concentration (data not shown). Multiple shots were taken for each Zn(II) concentration. Experiments were conducted a minimum of three times with different solutions, and the resulting averages are reported. The Kinet-Assyst software package (HiTech) was used to analyze the data. The observed rate constants were obtained by fitting individual traces to monoexponentials. Further experimental details are available in the Supporting Information and in ref 33.

Cell Culture. Human embryonic kidney (HEK293-T, HEK) cells were plated on untreated glass coverslips coated with 0.2% gelatin for at least 1 h at room temperature and grown to 90% confluence in Dulbecco's modified eagle medium (DMEM) supplemented with 10% FCS, glutamine (2 mM), penicillin (100 units/mL), and streptomycin (100 $\mu\text{g}/\text{mL}$). The medium was removed and replaced with DMEM containing 1% serum prior to ZP treatment. DMSO stock solutions (1 mM) of ZP were diluted to 100 μM with DMEM and added to the cells in DMEM containing 1% FCS by bath application for a final dye concentration of 10 μM . The cells were incubated with the probe for 2 h at 37 °C and under 5% CO₂, washed with serum-free DMEM (2 \times 2 mL), and bathed in serum-free DMEM (2 mL) before imaging. Stock solutions of Zn(II)/pyrithione (1:2 Zn(II)/pyrithione ratio prepared from ZnCl₂ and sodium pyrithione, 10 mM) and *N,N',N'',N'''*-tetrakis(2-picolyloxy)ethylenediamine (TPEN, 40 mM) in DMSO were diluted 10- and 40-fold with DMEM prior to cell treatment.

Hippocampal Slice Preparation. The whole brains of 90-day-old female Sprague–Dawley rats were removed. The hippocampi

were dissected on ice, cut into \sim 200 to \sim 400 μm thick slices and washed twice with Zn(II)-free Krebs's ringer buffer (literature protocol).³⁸ The slices were incubated with 10 μM dye in Zn(II)-free Krebs's ringer buffer ($T = 37$ °C, 5% CO₂) for 10–20 min, washed thoroughly with the Zn(II)-free buffer, and transferred to a glass-bottom imaging dish with a minimum volume of buffer for imaging.

Confocal Fluorescence Microscopy. A Zeiss LSM510 laser scanning microscopy system, based on an Axiovert 200M inverted fluorescence microscope, was used for confocal fluorescence imaging. The microscope was equipped with an argon ion laser ($\lambda_{\text{ex}} = 488$ nm), 10 \times or 63 \times objective lens, and a 505 nm long pass emission filter. During the imaging experiments, the samples were kept on the microscope stage in a CTI-3700 incubator set at 37 °C under 5% CO₂. Additions of Zn(II)/pyrithione and TPEN solutions to the biological samples were performed directly on the microscope stage by bath application. The Metamorph software package was used for quantification.

Results and Discussion

Syntheses. Sensors ZP9 and ZP10 were prepared by a convergent route that involves the combination of an asymmetrical aldehyde-functionalized fluorescein and the aniline-based ligand moiety.²⁶ Scheme 1 depicts the syntheses of ligand fragments **8** and **11** and the assemblies of sensors ZP9 and ZP10. The pyridyl-amine-pyrrole ligand **4** was prepared from 2-(aminomethyl)pyridine and 2-pyrrolicarboxaldehyde according to a literature procedure.³⁵ The *N*-methyl analogue, **5**, was obtained in an 82% yield by an analogous route. Combination of secondary amines **4** and **5** with 2-nitrobenzylbromide and base produced compounds **7** and **10** as yellow solids in high yields following purification by column chromatography. Reduction of the nitro groups in **7** and **10** to amino groups by hydrogenation using Pd/C (10% activated) was efficient and afforded the aniline-derivatized ligand fragments **8** and **11** in 52 and 60% yields, respectively, following column chromatography.

The final assembly of sensors ZP9 and ZP10 followed previously described methods.²⁶ Schiff base condensation of aldehyde **6** and the aniline-derivatized ligands in EtOAc yielded intermediates **9** and **12**. The reduction of the imines by NaB(OAc)₃H in 1,2-dichloroethane occurred readily and could be monitored by changes in solution clarity and color. The solutions of the fully reduced species prepared in this investigation were orange-yellow and clear. Sensors ZP9 and ZP10 were purified by preparative TLC on RP silica gel and obtained as orange solids in moderate yields. An aniline-derivatized fluorescein, **13**, was prepared analogously as shown in Scheme 2.

Effect of pH on Sensor Emission. Photoinduced electron transfer (PET) sensors are often proton sensitive.^{39,40} We therefore investigated the effect of pH on the emission properties of ZP9 and ZP10; representative titrations are

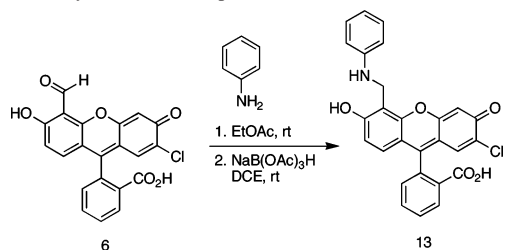
(38) Qian, W.-J.; Gee, K. R.; Kennedy, R. T. *Anal. Chem.* **2003**, *75*, 3468–3475.

(39) de Silva, A. P.; Gunaratne, H. Q. N.; Gunnlaugsson, T.; Huxley, A. J. M.; McCoy, C. P.; Rademacher, J. T.; Rice, T. E. *Chem. Rev.* **1997**, *97*, 1515–1566.

(40) Callan, J. F.; de Silva, A. P.; Magri, D. C. *Tetrahedron* **2005**, *61*, 8551–8588.

(37) Lim, M. H.; Xu, D.; Lippard, S. J. *Nat. Chem. Biol.* **2006**, *2*, 375–380.

Scheme 2. Synthesis of Compound 13



given in Figure 2. The pH profiles of these probes are essentially identical, as expected given their structural similarity. Both sensors show ~ 2 -fold fluorescence enhancement as the pH is lowered from ~ 12 to ~ 6 , and fluorescence quenching occurs in more acidic solutions. These titrations reveal two protonation events that alter sensor emission significantly and are assigned to aniline ($pK_{a1} = 7.2$, ZP9; 7.0, ZP10) and fluorescein ($pK_{a2} = 5.0$, ZP9; 4.8, ZP10) protonation (Table 4.1). Nitrogen protonation often causes fluorescence enhancement in PET-based sensors, which accounts for pK_{a1} . Fluorescein itself is pH sensitive,⁴¹ and its emission is quenched at low pH, which forms the basis for the assignment of pK_{a2} . To understand the latter transition further, we employed optical absorption spectroscopy, and representative spectra for ZP9 are given in Figure S1 (Supporting Information). The optical absorption spectra of fluorescein in its various protonation states are distinctive. The spectra of ZP9 at a pH of >7 are indicative of the fluorescein dianion, whereas those at lower pH, with peaks at ~ 484 and 459 nm of similar and significantly lower molar absorptivity, signal phenol protonation and formation of the fluorescein monoanion.⁴¹ Based on these observations, we propose the protonation equilibria for ZP9 and ZP10 shown in Scheme 3 where “observed” indicates the transitions detected by fluorimetric titrations. On the basis of literature studies of 2',7'-dichlorofluorescein,⁴² we expect protonation of the keto group to occur at a pH of <1 .

The preceding two-component pK_a analysis suggests that protonation of the tertiary amines in ZP9 and ZP10 has little influence on fluorophore emission. Investigation of the pH-dependent emission of **13** generally supports this notion (Figure 2, Scheme S1). The emission of **13** shows essentially no change as the pH is lowered from ~ 12 to ~ 7.5 . A ~ 2 -fold fluorescence increase occurs between pH ~ 7.5 and ~ 5.4 , which returns a pK_{a1} value of 6.1 assigned to aniline nitrogen protonation. A further decrease of the pH causes quenching, with a pK_{a2} of 4.7. Optical absorption spectroscopy reveals that phenol protonation is responsible for this transition (Figure S1). The pH-dependent fluorescent profiles of both ZP probes and **13** are therefore similar in the following ways: (i) the maximum emission is quenched by 40–50% at pH 12; (ii) this weak background emission is approximately doubled as the pH is lowered to ~ 6 , and (iii) further acidification causes the emission to decrease substantially and with comparable pK_a values. Some differences

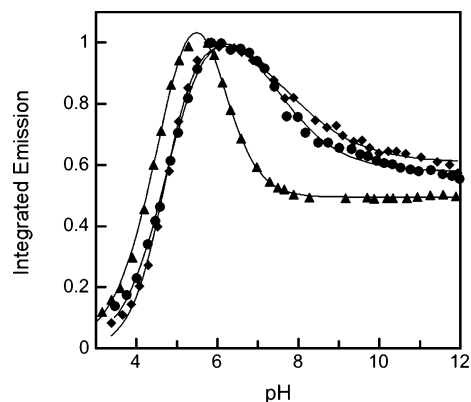


Figure 2. Effect of pH on the emission of ZP9 (●), ZP10 (◆), and **13** (▲). Solutions of $1 \mu\text{M}$ dye were prepared in 10 mM KOH, 100 mM KCl (pH ~ 12). The pH was lowered in increments of ~ 0.25 by the addition of aqueous HCl, and the fluorescence spectrum was recorded at each point. The data were integrated, normalized, and plotted against pH. Excitation was provided at 495 (ZP9, ZP10) or 500 (**13**) nm and $T = 25^\circ\text{C}$.

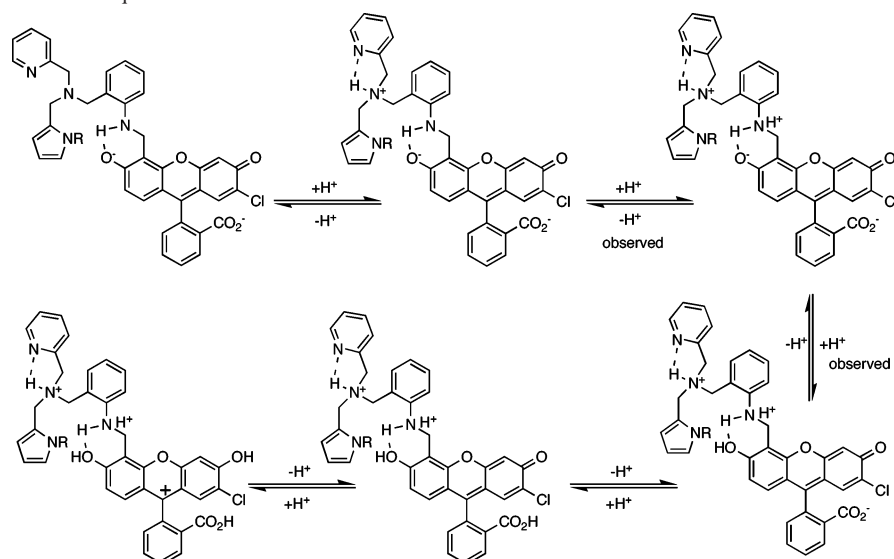
in the pK_{a1} transition for **13** and ZP9 and ZP10 are also worth noting. In contrast to the stable emission from **13** over the pH range from ~ 12 to ~ 7.5 , ZP9 and ZP10 both show an ~ 1.5 -fold increase in integrated emission, which may suggest that tertiary amine protonation has some contribution to the observed fluorescence enhancement in this pH regime. Given that a two-parameter model returns an excellent fit ($r = 0.997$ for both ZP9 and ZP10), we opted not to incorporate a third variable, but we acknowledge that some contribution from tertiary amine protonation may influence emission in this pH range. Nevertheless, any such effect is small because these compounds, and other aniline-based sensors with²¹ and without³³ tertiary-amine-based ligand appendages, have similar Φ_{free} values at neutral pH (vide infra).

Spectroscopic Properties of ZP9 and ZP10. Table 1 details the spectroscopic characterization of ZP9 and ZP10, in addition to data for structurally related Zn(II) sensors. ZP9 and ZP10 differ from one another only in the substitution on the pyrrole nitrogen atom, and we anticipated that they would exhibit comparable features. The data in Table 1 generally support this expectation. ZP9 and ZP10 both have fluorescein-dominated emission spectra with $\lambda_{\text{max}} \approx 520$ nm and $\Phi_{\text{free}} < 0.1$ (50 mM PIPES, 100 mM KCl, pH 7). These quantum efficiencies are in the range of most asymmetrical fluorescein-based metal ion sensors that employ aniline-based chelates designed by our group. This comparison suggests that the aniline-based ZP platform is relatively insensitive to variations in the tertiary amine fragment. Photophysical characterization of compound **13**, which has $\Phi_{\text{free}} = 0.06$ (50 mM PIPES, 100 mM KCl, pH 7), further substantiates this claim and reveals that fluorescence quenching observed in aniline-derivatized fluoresceins can be attributed to the aniline moiety with little, if any, contribution from the tertiary amine fragment. Such insensitivity to ligand variations is an advantage toward achieving a sensor series with similar photophysical properties and varied affinity or Zn(II) selectivity.

The fluorescence responses of ZP9 and ZP10 to Zn(II) are shown in Figure 3. Solutions of ZP9 and ZP10 exhibit immediate fluorescence turn-on following Zn(II) addition.

(41) Sjöback, R.; Nygren, J.; Kubista, M. *Spectrochim. Acta, Part A* **1995**, *51*, L7-L21.

(42) Leonhardt, H.; Gordon, L.; Livingston, R. *J. Phys. Chem.* **1971**, *75*, 245–249.

Scheme 3. Proposed Protonation Equilibria for ZP9 and ZP10^a

^a Observed indicates that the protonation event is detectable by fluorimetric titration in the pH range of ~ 12 to ~ 3 .

Table 1. Spectroscopic and Thermodynamic Data for Several Asymmetrical Zn(II) Sensors^a

	absorption λ (nm), ϵ ($\times 10^4$ M ⁻¹ cm ⁻¹)		emission λ (nm), Φ^b		pK _a ^c (N)	pK _a ^d	ref
	unbound	Zn(II)	unbound	Zn(II)			
ZP4 ^e	506, 6.1	495, 6.7	521, 0.06	515, 0.34	7.2	4.0	21
ZP9	505, 5.1	495, 4.4	526, 0.02	521, 0.41	7.2	5.0	this work
ZP10	506, 5.5	497, 4.5	523, 0.08	516, 0.33	7.0	4.8	this work
ZS4	507, 8.1	495, nd	522, 0.12	520, 0.50	7.6	5.1	32
ZQ1	505, 6.9	498, 7.0	524, 0.024	524, 0.78	6.1	5.0	33

^a Measurements were performed at pH 7 in 50 mM PIPES, 100 mM KCl buffer (except for pK_a determination). ^b Reported quantum yields are based on fluorescein ($\Phi = 0.95$ in 0.1 N NaOH, ref 36). ^c The pK_a value assigned to protonation of the aniline nitrogen atom. ^d The pK_a value assigned to phenol protonation. ^e See Figure 1 and Scheme 1 for nomenclature.

Both sensors give full emission enhancement in the presence of > 10 equiv of Zn(II) with $\Phi_{Zn} > 0.30$ (50 mM PIPES, 100 mM KCl, pH 7) and with ~ 12 - and ~ 7 -fold turn-on for ZP9 and ZP10, respectively. Blue shifts in both absorption and emission maxima occur as a result of Zn(II) binding, indicative of Zn(II) coordination to the phenol group. The absorption properties of ZP9 and ZP10, which are dominated by the fluorescein chromophore, are also listed in Table 1 and follow expected trends. Figure S2 includes representative absorption spectra for the free and Zn(II)-bound sensors and the corresponding difference spectra, which show absorption decreases at ~ 511 , 297, and 249 nm and increases at 461 and 490 nm. These features and the hypsochromic shift of A_{max} with Zn(II) coordination are consistent with those of previously reported ZP sensors.^{20,22,26}

Thermodynamics and Kinetics of Zn(II) Binding to ZP9 and ZP10. Table 2 summarizes the thermodynamic and kinetic parameters for Zn(II) coordination to ZP9 and ZP10. Both sensors were designed to bind Zn(II) with 1:1 stoichiometry, and Job plots are given in Figure S3. Fluorimetric titrations reveal that ZP9 has an apparent zinc complex K_d value of 0.69 ± 0.04 μ M (Fig. S4). This value is approximately 3 orders of magnitude higher than those for the parent ZP sensors ($K_{d1} < 1$ nM),²¹ ~ 1.5 orders of magnitude

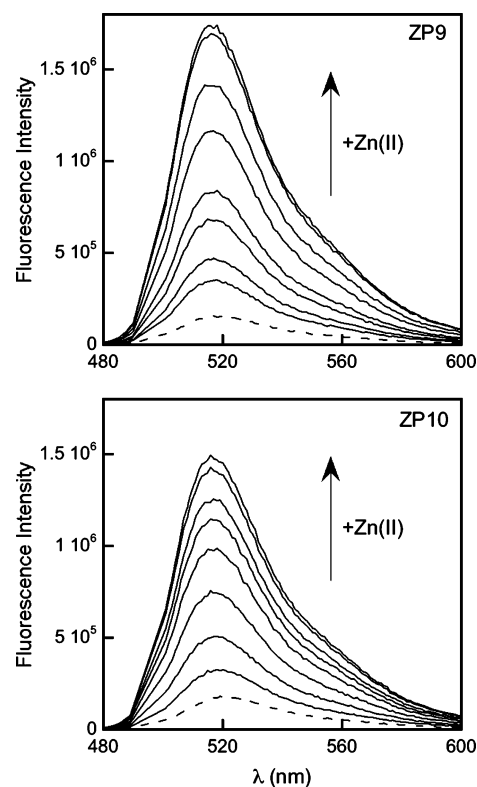


Figure 3. Fluorescence response of ZP9 and ZP10 to Zn(II) at pH 7 (50 mM PIPES, 100 mM KCl). (top) The dashed line indicates the emission from a 1 μ M solution of ZP9. The solid lines represent the fluorescence enhancement that occurs in the presence of 0.17, 0.33, 0.66, 1, 2, 4, 7, and 30 μ M Zn(II). (bottom) The dashed line indicates the emission from a 1 μ M solution of ZP10. The solid lines represent the fluorescence enhancement that occurs in the presence of 0.33, 1, 2, 4, 6, 8, 20, and 30 μ M Zn(II). Excitation was provided at 497 nm and $T = 25$ $^{\circ}$ C.

higher than that of Fluo-3N ($K_d = 15$ nM),⁴³ a commercially available Zn(II) sensor that employs a modified BAPTA chelate, and similar to the K_d values of Me₄ZP1 ($K_{d1} = 0.63$ μ M)³¹ and ZnAF-3 ($K_d = 0.79$ μ M).⁶ Substitution of the

(43) Gee, K. R.; Zhou, Z.-L.; Qian, W.-J.; Kennedy, R. *J. Am. Chem. Soc.* **2002**, *124*, 776–778.

Table 2. Kinetic Parameters and Dissociation Constants for ZP9 and ZP10^a

	k_{on} ($\text{M}^{-1} \text{s}^{-1}$) ^b 4.3 °C	k_{on} ($\text{M}^{-1} \text{s}^{-1}$) ^c 25 °C	K_{d} (μM) ^d 25 °C	$\sim k_{\text{off}}$ (s^{-1}) ^e 25 °C	ΔH^{\ddagger} (kcal mol^{-1})	ΔS^{\ddagger} ($\text{cal mol}^{-1} \text{K}^{-1}$)
ZP9	$3.00 \pm 0.09 \times 10^5$	$2.2 \pm 0.1 \times 10^6$	0.69 ± 0.04	1.5	14.4 ± 0.1	18.3 ± 0.9
ZP10	$2.04 \pm 0.04 \times 10^5$	$2.1 \pm 0.1 \times 10^6$	1.9 ± 0.2	4.0	14.6 ± 0.1	20.3 ± 2.0

^a All measurements were made at pH 7 (50 mM PIPES, 100 mM KCl). ^b Experimentally determined values for k_{on} at 4.3 ± 0.1 °C. ^c Experimentally determined k_{on} at 25 ± 0.1 °C from temperature-dependent studies. ^d Dissociation constants obtained experimentally by fluorimetric titration at 25 ± 1 °C. ^e Calculated k_{off} at 25 °C. ^f Activation parameters were determined over a temperature range from ~ 4 to ~ 40 °C.

pyrrole with *N*-methylpyrrole further increases the K_{d} value to 1.9 ± 0.2 μM (Figure S3). Given the spectroscopic similarities between ZP4, ZP9, and ZP10, we anticipate that their parallel use for biological imaging will be of benefit and will allow for bracketing relative Zn(II) concentrations in the sub-nanomolar to low-micromolar range, the latter being midrange.

Stopped-flow kinetics investigations were conducted to determine the association rates, measured by fluorescence turn-on, of Zn(II) binding to ZP9 and ZP10. Representative plots of k_{obs} versus Zn(II) concentration ($T = 4.3$ °C) yield second-order rate constants of $3.00 \pm 0.09 \times 10^5$ (ZP9) and $2.04 \pm 0.04 \times 10^5 \text{ M}^{-1} \text{ s}^{-1}$ (ZP10) (Table 2, Figure S5). The smaller k_{on} value for ZP10 may result from a steric effect caused by the *N*-methyl group on the pyrrole moiety. Temperature-dependent studies reveal k_{on} values of $> 2 \times 10^6 \text{ M}^{-1} \text{ s}^{-1}$ at 25 °C (Table 2). These association rates indicate rapid Zn(II) complexation and are of similar magnitude to the k_{on} values for DPA-based ZP ($3.3\text{--}5.2 \times 10^6 \text{ M}^{-1} \text{ s}^{-1}$, $T = 25$ °C)³³ and ZnAF family members ($1.3\text{--}3.1 \times 10^6 \text{ M}^{-1} \text{ s}^{-1}$, $T = 25$ °C).¹² The calculated k_{off} values for ZP9 and ZP10 are ~ 1.5 and $\sim 4.0 \text{ s}^{-1}$, respectively, at $T = 25$ °C, which indicates significantly more rapid Zn(II) dissociation as compared to ZP sensors with the DPA chelate ($2.3\text{--}3.4 \times 10^{-3} \text{ s}^{-1}$, $T = 25$ °C).³³ This feature may be important for imaging Zn(II) flux during signaling events.

Variable-temperature experiments were performed over the range from ~ 4 to ~ 40 °C, and representative Eyring plots are given in Figures S6 and S7. The values for the activation enthalpies, ΔH^{\ddagger} , are 14.4 ± 0.1 (ZP9) and 14.9 ± 0.6 (ZP10) kcal mol^{-1} and indicate a low activation barrier and fast association. The activation enthalpies, ΔS^{\ddagger} , are 18.3 ± 0.9 (ZP9) and 20.3 ± 2.0 (ZP10) $\text{cal mol}^{-1} \text{K}^{-1}$. Positive values were previously observed³³ for selected ZP and QZ sensors (Table 2) and may reflect the dissociation of water molecules or buffer components from the Zn(II) coordination sphere in the rate-determining step.

Selectivity of ZP9 and ZP10 for Zn(II). Figure 4 details the selectivity of ZP9 for Zn(II), and the data for ZP10 are comparable. Because they provide nitrogen-rich coordination spheres, ZP9 and ZP10 are selective for Zn(II) over millimolar concentrations of K(I), Na(I), Ca(II), and Mg(II). Of the divalent first-row transition metal ions considered, these sensors are selective for Zn(II) over both Mn(II) and Fe(II). The selectivity for Zn(II) over Fe(II) is a significant advantage relative to ZP1–8 and similar to the behavior observed for ZS4. Substitution of one pyridyl group from the DPA unit with another moiety routinely conveys selectivity for Zn(II) over Fe(II). The data presented in Figure 4 also reveal that the pyrrole-containing sensors are selective

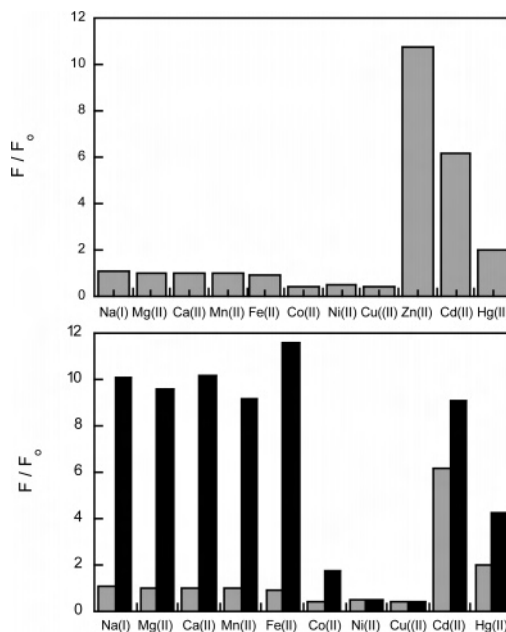


Figure 4. Selectivity of ZP9 for Zn(II) in the presence of other cations. (top) Fluorescence response of 1 μM ZP9 to 50 equiv of the cation of interest. The response (F) is normalized with respect to the emission of the free dye (F_0). (bottom) The fluorescence response of the solutions depicted in the top plot to Zn(II). The gray bars correspond to the bars in the top plot. The black bars indicate the normalized fluorescence response of the solutions immediately after introduction of 50 μM Zn(II). Excitation was provided at 495 nm. The responses of ZP9 and ZP10 to Zn(II) are also unaffected by millimolar concentrations of Na(I), K(I), Mg(II), and Ca(II).

for Zn(II) over its Group 12 congeners Cd(II) and Hg(II). This feature is an improvement over thioether-containing ZS sensors, which preferentially bind Hg(II) over Zn(II), and can be rationalized with the hard–soft acid–base (HSAB) principle, whereby sensors with nitrogen-rich chelates preferentially coordinate to Zn(II), whereas those with a thioether group bind Hg(II) more tightly.

Biological Imaging Applications. Given the fluorescence properties and Zn(II) affinities of ZP9 and ZP10, we initiated studies of their distribution and Zn(II) response in biological samples. Our initial expectations were based on previous biological imaging conducted with ZP4. Early studies with this probe showed that it selectively labels damaged neurons in brain tissue,^{21,34} and subsequent work in our laboratory with a basic tissue culture room microscope suggested that ZP4–6 do not readily enter cultured cells.²⁶ From these observations, ZP4 and its derivatives were assumed to be cell impermeable and useful for extracellular imaging. Given the structural similarities between ZP4 and the pyrrole derivatives described in this work, we reasoned that ZP9 and ZP10 would similarly be unable to penetrate the cell membrane without modification. We therefore prepared ZP9-

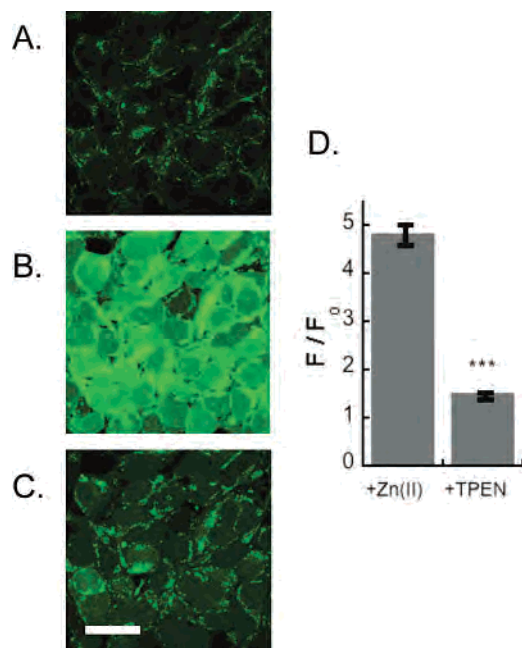
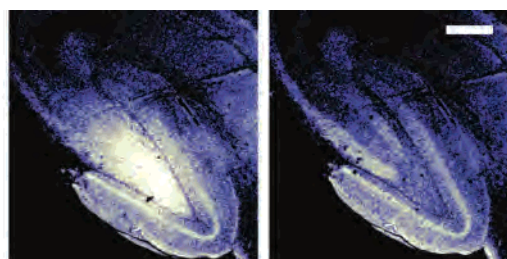


Figure 5. (A) Confocal fluorescence imaging of HEK293-T cells treated with ZP9 (10 μ M, 2 h, $T = 37^\circ\text{C}$, 5% CO_2). (B) Fluorescence images obtained following treatment with 1:2 ZnCl_2 /pyrithione (50 μ M, 10 min, $T = 37^\circ\text{C}$, 5% CO_2). (C) Fluorescence decrease observed following incubation with TPEN (50 μ M, 10 min, $T = 37^\circ\text{C}$, 5% CO_2). The scale bar indicates 25 μ m. (D) Quantification of the fluorescence rise and fall resulting from Zn(II) and TPEN treatments, respectively. The data (F) are normalized with respect to cells treated only with ZP9 (F_0). A total of 32 cells were quantified and *** indicates $p < 0.001$ (Mann–Whitney test). The error bars represent the standard error of the mean.

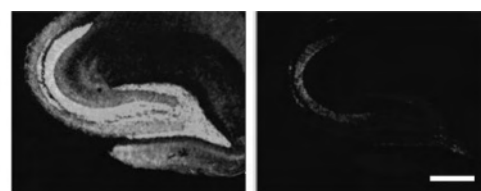


ZP9	+	+
TPEN	-	+

Figure 6. Confocal fluorescence images of an acute hippocampal slice from an adult female Sprague–Dawley rat. (left) The hippocampal slice was incubated with 10 μ M ZP9 for 10 min ($T = 37^\circ\text{C}$, 5% CO_2) in Zn(II)-free Krebs’ ringer buffer and washed thoroughly before imaging. Bright fluorescence is observed in the dentate gyrus region. (right) A fluorescence decrease is observed in the dentate gyrus following the addition of 50 μ M TPEN (5 min, $T = 37^\circ\text{C}$, 5% CO_2). The scale bar indicates 0.5 mm.

Piv by reaction of ZP9 with excess pivalic anhydride in the presence of base (Scheme S2). This approach, which affords the lipophilic lactone isomer of fluorescein, is commonly used for delivering an otherwise impermeable probe into cells.

Preliminary control studies suggested otherwise. Laser scanning confocal microscopy revealed that HEK cells treated with either ZP9 or ZP9-Piv exhibited intracellular staining. Further work definitively showed that ZP9 can enter cells and respond to exogenously added Zn(II), delivered by addition of the cell-permeable ionophore pyrithione. Representative images are given in Figure 5. Quantification of



ZP4	+	+
TPEN	-	+

Figure 7. Confocal fluorescence images of an acute hippocampal slice from an adult female Sprague–Dawley rat. (left) The hippocampal slice was incubated with 10 μ M ZP4 for 20 min ($T = 37^\circ\text{C}$, 5% CO_2) in Zn(II)-free Krebs’ ringer buffer and washed thoroughly before imaging. Bright fluorescence is observed in the dentate gyrus and CA3 regions. (right) A fluorescence decrease is observed in the dentate gyrus following the addition of 50 μ M TPEN (20 min, $T = 37^\circ\text{C}$, 5% CO_2). The scale bar indicates 0.5 mm.

the response indicates a ~ 5 -fold intracellular fluorescence enhancement following a 2 h dye incubation period and treatment with 5 equiv of Zn(II)/pyrithione. Addition of the cell-permeable chelator TPEN reversed the fluorescence increase to within 20% of the baseline value, which confirms that the fluorescence increase results from Zn(II) coordination and not some other phenomena, such as a proton flux or sensor photoactivation.

On the basis of our knowledge of ZP4, the behavior of ZP9 was a surprise. We concluded that relative incubation time is a key factor when defining the permeability of a probe and that an “appropriate” incubation time will also depend on the type of cell or tissue under study. An incubation time of only ~ 1 min was employed during the first experiments conducted with ZP4 in samples of brain tissue,²¹ which was presumably too short for the probe to enter healthy cells. We therefore investigated ZP4 staining of cultured HEK cells in detail and observed a distribution and response comparable to that of ZP9.⁴⁴ These studies point to the need for caution when designating a given sensor as intra- or extracellular and the necessity for rigorous control experiments.

Knowing that ZP4 and ZP9 can penetrate cell membranes and respond to Zn(II) *in vivo*, we sought to employ these probes to detect endogenous Zn(II) pools. We therefore treated acute hippocampal slices from adult rat brain with 10 μ M ZP4 or ZP9 for 10–20 min ($T = 37^\circ\text{C}$, 5% CO_2). Figure 6 shows the confocal images obtained for a representative slice treated with ZP9 and subsequently with 50 μ M TPEN. The dentate gyrus region, which contains glutamatergic neurons rich in vesicular zinc, is illuminated, and the signal is reversed with TPEN addition, which indicates that ZP9 ($K_d < 1 \mu\text{M}$) can detect endogenous Zn(II) in this region. ZP4 ($K_d < 1 \text{nM}$) also stains the Zn(II)-rich regions of the mammalian hippocampus (Figure 7). We note that optical z -sectioning of a ZP treated hippocampal slice confirms that the sensor has indeed penetrated the tissue (Figure S8). The ZP4 staining pattern differs significantly from those first obtained with a ~ 1 min incubation (room temperature, 3 h after slicing),²¹ which reflects one or more variations in the slice preparation and staining protocols. During the course of our work, ZP4 permeability was

(44) Nolan, E. M.; Frederickson, C. J.; Lippard, S. J. Unpublished results.

reported in hippocampal slices (0.5–3 h incubation) in a study of synaptic activation.⁴⁵

Summary and Perspectives

Investigations of ZP9 and ZP10 reveal several important facets of zinc sensor design and biological application. Incorporation of pyrrole groups affords a new strategy for increasing the Zn(II) dissociation constant and improving Zn(II) selectivity relative to sensors that use the DPA chelate. Through consideration of compound **13**, we determined that the fluorescence quenching of aniline-based sensors is primarily, if not completely, caused by the aniline moiety itself. This observation is an important one and suggests that systematic modification of this sensor platform, via changes in the groups of the tertiary amine unit, will afford a series of Zn(II) sensors with comparable optical properties that span a range of dissociation constants. Along these lines, we anticipate that parallel use of ZP4 and ZP9 for biological imaging will be of benefit and will allow for bracketing relative Zn(II) concentrations in the nanomolar range. Finally,

(45) Kay, A. R.; Tóth, K. *J. Neurophysiol.* **2006**, *95*, 1949–1956.

confocal imaging studies with ZP9 were particularly revealing and showed that aniline-based probes are cell permeable. As a result of this observation and subsequent studies, we revise our original claim that ZP4²¹ and its derivatives are exclusively extracellular Zn(II) sensors.

Acknowledgment. This work was supported by Grant GM65519 from the National Institute of General Medical Sciences. Spectroscopic instrumentation at the MIT DCIF is maintained by funding from NIH Grant 1S10RR13886-01 and NSF Grants CHE-9808061, CH3-9808063, and DB19729592. M.S. is an Investigator of the Howard Hughes Medical Institute. M.E.R. thanks the Undergraduate Research Opportunities Program at MIT for partial financial support. E.M.N. thanks the Whitaker Health Science Fund for a graduate fellowship, Strem Chemicals, Inc. for a gift of ZP4, and Mr. J. W. Ryu and Mr. D. P. Seeburg for assistance with the ZP4 slice experiment.

Supporting Information Available: Schemes S1–S2, Figures S1–S8, and representative ¹H NMR spectra. This material is available free of charge via the Internet at <http://pubs.acs.org>.

IC061137E